Interleukin-10 is a Critical Regulator of White Matter Lesion Containment Following Viral Induced Demyelination

Shweta S. Puntambekar,[1] David R. Hinton,[2] Xinghua Yin,[1] Carine Savarin,[1] Cornelia C. Bergmann,[1] Bruce D. Trapp,[1] and Stephen A. Stohlman[1*]

Neurotropic coronavirus induces an acute encephalomyelitis accompanied by focal areas of demyelination distributed randomly along the spinal column. The initial areas of demyelination increase only slightly after the control of infection. These circumscribed focal lesions are characterized by axonal sparing, myelin ingestion by macrophage/microglia, and glial scars associated with hypertrophic astrocytes, which proliferate at the lesion border. Accelerated virus control in mice lacking the anti-inflammatory cytokine IL-10 was associated with limited initial demyelination, but low viral mRNA persistence similar to WT mice and declining antiviral cellular immunity. Nevertheless, lesions exhibited sustained expansion providing a model of dysregulated white matter injury temporally remote from the acute CNS insult. Expanding lesions in the absence of IL-10 are characterized by sustained microglial activation and partial loss of macrophage/microglia exhibiting an acquired deactivation phenotype. Furthermore, IL-10 deficiency impaired astrocyte organization into mesh like structures at the lesion borders, but did not prevent astrocyte hypertrophy. The formation of discrete foci of demyelination in IL-10 sufficient mice correlated with IL-10 receptor expression exclusively on astrocytes in areas of demyelination suggesting a critical role for IL-10 signaling to astrocytes in limiting expansion of initial areas of white matter damage.

Introduction

Plaque formation in the CNS of multiple sclerosis (MS) patients has been appreciated for over a century; however, how discrete plaques are restrained is poorly understood. Demyelination with no evidence of T cells as an early event in MS (Barnett and Prineas, 2004) and expanding lesions with little or no T cells in autologous bone marrow recipients (Metz et al., 1994) both suggest expansion may be regulated by intrinsic pathological processes. The focal nature of white matter lesions in MS patients is also observed in rodents with experimental autoimmune encephalomyelitis (EAE), spinal cord injury, and demyelination induced by gliatropic coronavirus infection (Bender and Weiss, 2010; Bergmann et al., 2006; Liedtke et al., 1998; Okada et al., 2006; Voskuhl et al., 2009), supporting a conserved regulatory mechanism that restrains lesion expansion. Astrocytes are implicated as a criti-

cal component, as glial scars formed by reactive astrocytes demarcate injured areas following trauma, spinal cord injury, neurodegenerative disease, and autoimmune disease, thus shielding adjacent healthy tissue from bystander damage (Cregg et al., 2014; Sofroniew and Vinters, 2010). Ablating astrocyte intermediate filaments or inducing apoptosis of dividing astrocytes attenuates gliosis as well as formation of discrete demyelination foci (Liedtke et al., 1998; Toft-Hansen et al., 2011). Similarly, elimination of Signal Transducer and Activator of Transcription (STAT)-3, required for signaling via interleukin (IL)-6, IL-10, leukemia inhibitory factor (LIF), and ciliary neurotropic factor (CNTF), specifically in astrocytes inhibits scar formation (Herrmann et al., 2008; Wanner et al., 2013). By contrast, abrogation of Suppressor of Cytokine Signaling (SOCS)-3 in astrocytes, thereby increasing STAT3 phosphorylation, limits lesion area,

enhances astrocyte migration, and improves functional recovery (Okada et al., 2006).

The anti-inflammatory cytokine IL-10 also provides neuroprotection by ameliorating demyelination caused by neurotropic coronavirus (Trandem et al., 2011) and reducing encephalomyelitis caused by Sindbis virus infection (Kulcsar et al., 2014). Although IL-10 decreases tissue damage at the cost of limiting pathogen control (Chen et al., 2012; Couper et al., 2008b; Holscher et al., 2000; Kullberg et al., 2002), the contribution and mechanisms by which of IL-10 ameliorates pathology varies dramatically with the type of infection, the target tissue and source of IL-10 (Couper et al., 2008a,b; Kullberg et al., 2002; Lund et al., 2008; Sun et al., 2009, 2011). IL-10 production at sites of inflammation commonly limits macrophage and dendritic cell maturation, resulting in suppression of T cell function (Couper et al., 2008a; Fahey and Brooks, 2010). However, during encephalomyelitis caused by glia tropic coronavirus designated JHMV, IL-10 deficiency increases demyelination and lethality, despite accelerated virus control in the CNS and quiescence of antiviral T cell function (Lin et al., 1998; Trandem et al., 2011). These outcomes represented an intriguing conflict, as delayed viral control generally correlates with enhanced demyelination in this model (Lin et al., 1999; Ramakrishna et al., 2002). Demyelination induced by sublethal neurotropic mouse hepatitis virus strains, including JHMV, require both oligodendroglia infection and adaptive immunity (Bender and Weiss, 2010; Bergmann et al., 2004, 2006; Wu et al., 2000). Lesions containing macrophages and microglia develop prominently after virus control (Bergmann et al., 2006; Templeton et al., 2008), but lesion formation is independent of both IL-17 and infiltrating monocytes, distinct from EAE (Kapil et al., 2009; Savarin et al., 2010; Xue et al., 1999). Furthermore, IL-10 is primarily secreted by CD4$^+$ T cells within the JHMV infected CNS (Puntambekar et al., 2011), although IL-10 may be secreted by numerous cell types in other models (Couper et al., 2008a; Saraiva and O'Garra, 2010).

To better understand the cellular events underlying the protective effects of IL-10 on demyelination we performed a detailed kinetic analysis of viral control, persisting virus, and lesion formation in JHMV infected WT and IL-10$^{-/-}$ mice. Accelerated viral control in the absence of IL-10 initially resulted in limited demyelination. However, in contrast to relatively stable lesions with well demarcated borders in WT mice, lesion areas increased in the absence of IL-10 without evidence of viral recrudescence or altered cellular immunity. The expanding lesions exhibited ill-defined borders and lacked elongated interdigitating processes associated with scar formation in WT mice, despite the presence of hypertropic astrocytes. In the absence of IL-10, lesions were also characterized by large foamy cells, axonal sparing, and a partial loss

of macrophage/microglia exhibiting an acquired deactivation phenotype. Expanding lesion formation, temporally remote from the viral insult, is thus reminiscent of the epidemiological association of MS with an early insult, possibly an infection. Moreover, the data suggest a novel astrocyte dependent mechanism by which IL-10 contributes to stemming pathology within the CNS.

Materials and Methods

Mice and Virus Infection

C57BL/6 WT mice were purchased from the National Cancer Institute (Frederick, MD). IL-10 deficient mice on a C57BL/6 background (IL-10$^{-/-}$), purchased from The Jackson Laboratory (Bar Harbor, MA), were housed and maintained locally under pathogen free conditions. Mice were infected at 6 to 7 weeks of age by intracranial injection of 250 plaque forming units of the glia tropic mAb derived escape mutant of mouse hepatitis virus strain JHM (JHMV), designated V2.2-1 (Fleming et al., 1986). Infectious virus was determined in clarified supernatants of homogenized brains by plaque assay as described (Fleming et al., 1986). Plaques were counted after 48 h incubation at 37°C. All procedures were conducted under protocols approved by the Institutional Animal Care and Use Committee.

Isolation of CNS Cells and Enzyme Linked Immunosorbent Assay (ELISA)

Cells from the CNS were isolated by nonenzymatic homogenization and using 30%/70% Percoll (Pharmacia, Piscataway, NJ) step gradients as described (Bergmann et al., 1999; Kapil et al., 2009). Supernatants from the homogenates were stored at −80°C for virus titer determination and ELISA. Cells recovered from the Percoll interphase were washed with RPMI containing 25 mM HEPES and resuspended in FACS buffer (PBS containing 0.5% BSA). Cervical lymph nodes (CLN) were collected in cold RPMI supplemented with 25 mM HEPES, dissociated by passage through 70 µm cell strainers and washed as above. Viable cells were determined by Trypan blue exclusion and a minimum of 5×10^5 cells used for flow cytometric analysis.

IFN-γ in clarified brain supernatants was determined by ELISA as described (Kapil et al., 2009). Briefly, supernatants were added in triplicate to 96 well plates (Fischer Scientific) precoated with mouse antiIFN-γ mAb (1 µg/ml; R4-6A2; BD Biosciences) and blocked with 10% FBS in PBS. Following incubation overnight at 4°C, IFN-γ was detected using biotinylated anti-IFN-γ mAb (1 µg/ml; XMG1.2; BD Biosciences), avidin-horseradish peroxidase and 3,3′,5,5′-TMB substrate reagent set (BD Biosciences). Optical density was measured at 450 nm with a microplate reader (Bio-Rad Laboratories, Hercules, CA) and analyzed with SoftMax Pro software (Molecular Devices, Sunnyvale, CA).

Flow Cytometric Analysis

Cells were incubated with mouse serum and rat anti-mouse FcγIII/II mAb (2.4G2) (BD Biosciences, San Diego, CA) for 20 min on ice to minimize nonspecific binding. Cell type specific expression of

surface antigens (Ag) was determined by incubation with either phycoerythrin (PE)-, fluorescein isothiocyanate (FITC)-, phycoerythrin-peridinin chlorophyll protein (PerCP)-, or allophycocyanin (APC)-conjugated mAb specific for CD45 (30-F11), CD11b (M1/20), major histocompatibility complex (MHC) class II (IA/IE, 2G9), CD4 (RM4-5), and CD8 (53–6.7) (all from BD Biosciences, San Jose, CA) for 30 min on ice.

CNS derived T cells were analyzed for virus specific IFN-γ production by viral peptide stimulation (Kapil et al., 2009). CNS cells (~5 × 10^5) were incubated with 2 × 10^5 H-2^b EL4 cells with or without 0.5 μM S510 peptide for CD8^+ T cells, or with I-A^b expressing CHB3 cells with or without 5 μM M133 peptide for CD4^+ T cells. After 6 h stimulation at 37°C in RPMI supplemented with 10% FBS and 1 μl/ml golgi stop (BD Biosciences, San Jose, CA), cells were centrifuged, resuspended in FACS buffer, and stained for surface expression of CD4, CD8, and CD45. Cells were fixed and permeabilized using Cytofix/Cytoperm reagent (BD Biosciences, San Jose, CA) and intracellular IFN-γ detected by incubation with FITC-labeled anti-IFN-γ mAb (XMG1.2). Data were collected using a FACSCalibur flow cytometer (BD Biosciences, San Jose, CA) and analyzed using FlowJo (7.6.1) software (Tree Star, Ashland, OR).

Cytotoxic T Lymphocyte Assay

Cytolysis by virus specific CD8^+ T cells was analyzed using EL4 cells pulsed with H-2D^b restricted S510 peptide (de Aquino et al., 2014). Target cells were incubated with 0.5 μM S510 peptide for 2 h at 37°C, washed, and labeled with 2.5 μM carboxyflourescein succinimidyl ester (CFSE; Molecular Probes, Eugene, OR). Non-peptide treated control EL4 cells were labeled with 0.125 μM CFSE. Control and peptide pulsed targets were mixed at a 1:1 ratio, added to 96 well plates and incubated with CNS derived cells at various effector:target (E:T) ratios based on virus specific CD8^+ T cells measured using D^b/S510 MHC class I tetramers (Beckman Coulter, Fullerton, CA). After 6 h incubation at 37°C, the loss of CSFE labeled cells was determined using a FACSCalibur flow cytometer (BD Biosciences). Data were analyzed using FlowJo (7.6.1) software. Specific lysis of peptide pulsed target cells was calculated based on the following formula: [1-(ratio of targets only/ratio of target + T cells)] × 100.

Histopathological Analysis

Spinal cords were fixed in 10% Zinc formalin, divided into six sections corresponding to cervical, thoracic and lumbar regions and embedded in paraffin as described (de Aquino et al., 2014; Puntambekar et al., 2011). Sections were stained with hematoxylin and eosin (H&E) to visualize inflammation or Luxol Fast Blue (LFB) to visualize myelin. Viral Ag was detected by anti-JHMV mAb J.3.3 specific for the viral nucleocapsid (N) protein and visualized using immunoperoxidase labeled antimouse mAb (Vectastain-ABC kit, Vector Laboratories, Burlingame, CA) and 3,3-DAB (Sigma, St. Louis, MO) as chromogen. Sections from 6 levels per mouse were scanned with an AperioScanScope (Vista, CA) at 40×, digitally imaged at high resolution, and scored in a blind manner for inflammation, demyelination, and viral Ag. In addition, demyelination

within the white matter was quantified using Aperio software (Vista, CA). Representative fields for photomicroscopy were identified based on average score of all sections in each experimental group.

For confocal microscopy spinal cords from PBS perfused animals were embedded in Tissue-Tek OCT compound (Sakura Finetek, Torrance, CA) and snap frozen in liquid nitrogen. Tissues were sectioned onto Microfrost slides (Fisher Scientific, Florence, KY) at 10 μm and stored at −80°C. Prior to staining, slides were subjected to heat mediated Ag retrieval using 0.01M citrate buffer, pH 6.0, fixed with 4% paraformaldehyde for 20 min at room temperature, permeabilized with 0.1% Triton X 100 for 30 min at room temperature and blocked for 30 min at room temperature with a mixture of 10% normal goat serum (Atlanta Biologicals, Lawrenceville, GA) and 1% BSA (Sigma Aldrich, St. Louis, MO) in PBS. Primary Ab were applied in blocking solution overnight at 4°C. Areas of demyelination were identified using mouse anti-myelin proteolipid protein (PLP) mAb (Millipore, PLPC1,1:500). Microglia/macrophages were detected using rabbit anti-Iba1 polyclonal Ab (Wako, 019-19741, 1:300). Microglia/macrophage phenotypes were identified using rat anti-MHC class II mAb (Abcam, M5/114, 1:600), mouse anti-inducible nitric oxide synthase (iNOS) mAb (BD biosciences, 610330, 1:100) and rabbit anti-mannose receptor Ab (Abcam,1:600). Astrocytes were identified using rat anti-GFAP mAb (Invitrogen, 2.2B10, 1:300). IL-10R expression was detected using rabbit anti-IL-10Rα Ab (SantaCruz, C-20, 1:300). Tissues were incubated for 1 h at room temperature with alexa fluor goat anti-rabbit 488, alexa fluor goat anti-mouse 594 or alexa fluor goat anti-rat 594 (all from Invitrogen, 1:1000). Slides were mounted with Prolong Gold antifade reagent with DAPI (Invitrogen) and analyzed on a Leica TCS confocal microscope and Leica DM4000B fluorescence microscope.

For epon embedded sections animals were perfused with 4% paraformaldehyde and 2.5% glutaraldehyde in Sorensons phosphate buffer. Spinal cord segments were placed in fixative overnight, post fixed in Osmium tetroxide, and processed to Epon by standard procedures. Cross-sections of cervical, thoracic, and lumbar cord segments were cut on an ultramicrotome at a thickness of 1 micron and stained with toluidine blue.

Gene Expression

Spinal cords were homogenized in Trizol (Invitrogen) using a Tissue Lyzer and stainless steel beads (Qiagen, Valencia CA) and RNA isolated as described (de Aquino et al., 2014). Following DNase I treatment (DNA-free kit; Ambion, Austin, TX), cDNA was synthesized using Moloney murine leukemia virus (M-MLV) reverse transcriptase (Invitrogen) with oligo(dT) and random primers (Promega, Madison, WI). Quantitative real-time PCR (qRT-PCR) was performed using SYBR green master mix (Applied Biosystems, Foster City, CA) in triplicate on a 7500 Fast real-time PCR system (Applied Biosystems). PCR conditions were 10 min at 95°C followed by 40 cycles of 95°C for 15 s, 60°C for 30 s, and 72°C for 30 s. Real-time primer sequences were as follows: GAPDH sense, 5′-CATGGCCTTCCGTGTTCCTA-3′; GAPDH antisense, 5′-ATGCCTGCTTCACCACCTTCT-3′, JHMV N gene sense, 5′-CGCAGAGTATGGCGACGAT-3′; JHMV(N) antisense, 5′-GAGGTCCTAG
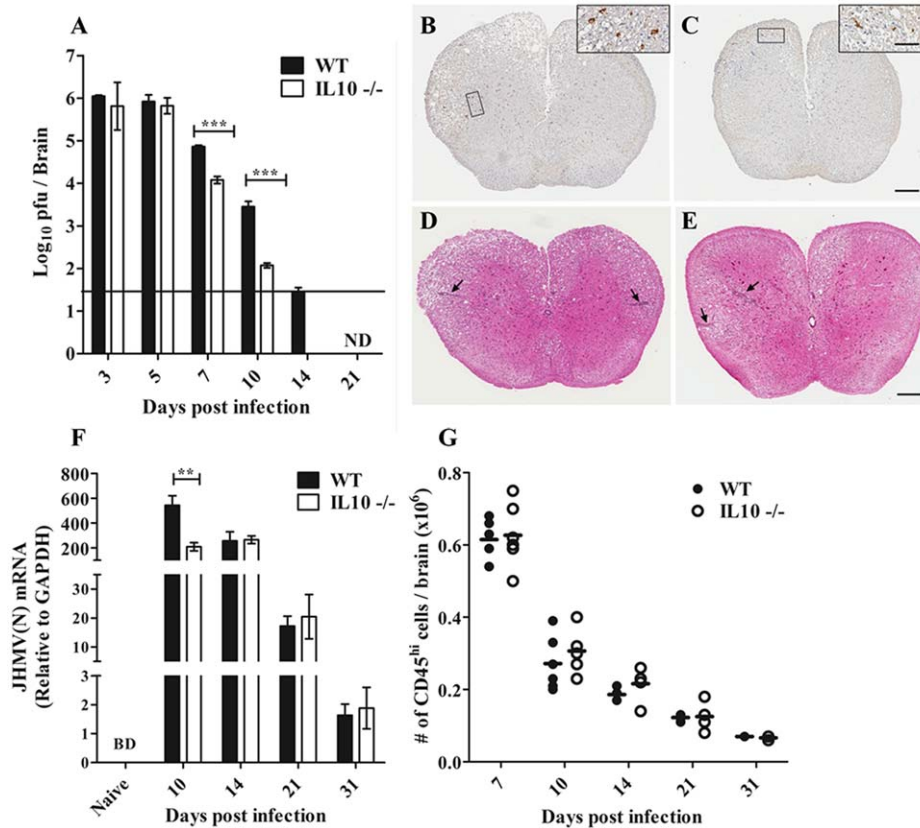
FIGURE 1: Enhanced viral control in the absence of IL-10 does not prevent persistence. (A) Infectious virus in the CNS at various times p.i. determined by plaque assay. Data represent three independent experiments with $n = 9$ mice per time point. Horizontal line represents the limit of detection. ND = not detected. Immunohistochemical localization of virus infected cells in spinal cords of (B) WT and (C) IL-10$^{-/-}$ mice at day 14 p.i. Infected cells have morphology typical of oligodendrocytes. Scale bar = 200 microns, Inset scale bar = 50 microns. Inflammatory foci in spinal cords (arrows) from infected (D) WT and (E) IL-10$^{-/-}$ mice at day 14.p.i. Scale bar = 200 microns (F) Expression of JHMV(N) mRNA in spinal cords of infected WT and IL-10$^{-/-}$ mice. Data represent two separate experiments and are expressed as mean ± SEM of 6 individual spinal cords per time point relative to GAPDH mRNA expression. (G) Total numbers of CD45^{hi} cells in brains of WT and IL-10$^{-/-}$ infected mice at various times p.i. Each data point represents an independent experiment with samples pooled from 3 to 4 mice per time point. ***$P < 0.0001$ determined by unpaired, two-tailed student's t-test.

TCTCGGCCTGTT-3′; Arginase-1 (Arg-1) sense, 5′-TGGGTG GATGCTCACACTGA-3′, Arg-1 antisense, 5′-CAGGTTGC CCATGCAGATT-3′; IL-1 receptor antagonist (IL-1Ran) sense, 5′-AGATAGACATGGTGCCTATTGACCTT-3′, IL-1Ran antisense, 5′-CATCTCCAGACTTGGCACAAGA-3′. For IFN-γ (Mm01168 134_m1) and GAPDH (Mm99999915_g1) expression levels were determined using Applied Biosystems gene expression arrays with Universal TaqMan Fast master mix (Applied Biosystems). PCR conditions were 20s at 95°C followed by 40 cycles of 95°C for 3 s and 60°C for 30 s. Transcript levels were calculated relative to the levels of the housekeeping gene GAPDH using the formula $2^{[CT\ (\text{GAPDH}) - CT(\text{target gene})]} \times 1,000$ where C_T is determined as the threshold cycle at which the fluorescent signal becomes significantly higher than that of the background.

Quantification and Statistical Analysis

Lesion area and total cell numbers were quantified using images acquired with a Leica DM4000B fluorescence microscope at 10× magnification. PLP stained lesions were outlined and the selected area quantified using the ImageJ/Fiji processing software. Cells of

interest within the area were counted manually. The total number of cells normalized to 1 mm^2 lesion area was calculated using the formula [(number of cells in lesion/total area of lesion)] × 10^5. Statistical analysis was performed using Microsoft excel and GraphPad Prism 5 Software. Individual groups were compared using the unpaired, two-tailed Student's t-test at a 95% confidence interval. A value of $P < 0.05$ was considered statistically significant.

Results

IL-10 Limits Viral Clearance

To resolve the discrepancy between IL-10 mediated control of tissue damage coupled with delayed virus control, pathogenesis was monitored longitudinally in WT and IL-10$^{-/-}$ mice infected with sublethal JHMV. CNS viral loads were initially similar in both groups, but were reduced more efficiently in IL-10$^{-/-}$ mice at days 7 and 10 post infection (p.i.) as the host exerts T cell mediated control (Fig. 1A). By day 14 p.i. infectious virus was still detectable in the CNS of some WT mice, but cleared from IL-10$^{-/-}$ mice (Fig. 1A), consistent

with less than 10% mortality in both groups. These data confirm that the anti-inflammatory cytokine IL-10 delays viral control within the CNS (Lin et al., 1998; Trandem et al., 2011).

JHMV initially replicates in brain, but rapidly spreads into the spinal cord where it preferentially infects and persists within oligodendrocytes (Kapil et al., 2012; Phares et al., 2014; Wang et al., 1992). Consistent with more efficient virus control in brain in the absence of IL-10, virus infected cells in spinal cord also appeared to be reduced (Fig. 1B,C). Moreover, similar morphology and distribution of virus infected cells indicated that viral tropism was not altered. Accelerated control of infectious virus in the absence of IL-10 suggested that viral persistence may also be reduced. However, although levels of the abundant viral mRNA encoding the N protein were reduced in IL-10$^{-/-}$ relative to WT spinal cords at day 10 p.i., they were similar in both groups thereafter (Fig. 1F). IL-10 deficiency also did not alter the extent or distribution of inflammatory foci in spinal cords (Fig. 1D,E). CNS recruitment of CD45^{hi} inflammatory cells was examined to support the notion that the anti-inflammatory properties of IL-10 (Couper et al., 2008a) did not alter cellular infiltrates. Indeed, IL-10 deficiency did not affect the accumulation of inflammatory cells at any time p.i. (Fig. 1G). Thus, despite an IL-10 dependent delay in clearance of infectious virus, IL-10 did not affect overall inflammation, viral tropism, or persistence.

IL-10 Preferentially Influences Virus Specific CD4$^+$ T Cells

To assess whether enhanced viral control correlated with increased T cell effector activity we measured IFN-γ as the primary T cell derived mediator of viral control (Bergmann et al., 2004; Parra et al., 1999; Stohlman et al., 2008). Indeed, IFN-γ levels within the CNS were elevated in the absence of IL-10 (Fig. 2A). Virus specific CD4$^+$ T cells within the CNS produce higher levels of IFN-γ as compared to CD8$^+$ T cells (Phares et al., 2010), although CD8$^+$ T cells are essential to control JHMV infection (Bergmann et al., 1999, 2004). To assess which T cell subset is responsible for enhanced IFN-γ levels in the absence of IL-10, numbers and function of virus specific T cells within the CNS were analyzed. Although total CD4$^+$ T cell numbers were similar in both groups at all times p.i., virus specific IFN-γ$^+$CD4$^+$ T cells were more abundant in the absence of IL-10 at day 7 p.i. (Fig. 2A), when virus control was initially apparent. In addition, mean fluorescent intensity (MFI) of the IFN-γ producing populations indicated CD4$^+$ T cells from the CNS of IL-10$^{-/-}$ mice produced more IFN-γ at the cellular level (Fig. 2B). To confirm that increased IFN-γ was mainly attributable to CD4$^+$ T cells, CD8$^+$ T cells were also analyzed. Neither the number of virus specific CD8$^+$ T cells detected by S510/H-2D^b tetramer staining (Fig. 2C), the percentage of virus specific CD8$^+$ T cells secreting IFN-γ, nor their relative MFI (data not shown) were altered in the absence of IL-10. Similarly, CD8$^+$ T cell cytolytic activity, also contributing to virus control (Bergmann et al., 2004), was similar (Fig. 2D). Overall, these data support the notion that IL-10 primarily inhibits control of infectious virus within the CNS by suppressing IFN-γ secretion specifically by CD4$^+$ T cells, albeit without affecting the level of viral persistence or CD8$^+$ T cell function.

IL-10 Limits Lesion Area

To determine how the accelerated virus reduction influenced tissue damage, the extent of demyelination in spinal cords was quantified. Because of the random distribution of focal lesions along the neuroaxis following JHMV infection, areas of demyelination were quantified in individual spinal cord sections representing six levels. In WT mice demyelination affected ∼8% of white matter by day 10 p.i. and then remained relatively constant (Fig. 3A). By contrast, demyelination was reduced by ∼50% at days 10 and 14 p.i. in IL-10$^{-/-}$ relative to WT mice. However, by day 31 p.i. demyelination had increased to ∼35% in the absence of IL-10 (Fig. 3A), representing a 3.5-fold increase relative to WT mice. Thus, despite ongoing viral control in the 2 week interval, damage to the white matter tracks could not be contained in the absence of IL-10.

The absence of viral recrudescence in infected IL-10$^{-/-}$ mice (Fig. 1) suggested that increased demyelination is independent of new foci initiated by sustained viral replication. Therefore, lesion area was measured to distinguish increased numbers of foci from increased size of individual lesions. Lesion area within spinal cords of infected WT mice increased ∼2-fold between days 14 and 21 p.i. and then remained relatively stable (Fig. 3B). Although lesion area in IL-10$^{-/-}$ spinal cords was initially decreased relative to WT controls, it progressively increased in the absence of IL-10 (Fig. 3B). These data contrast with the focal demarcated and relatively stable lesion area in WT mice between days 21 and 31 p.i. (Fig. 3B). Kinetic analysis of lesion area and percentage demyelination thus both revealed that increased demyelination in infected IL-10$^{-/-}$ mice is initially preceded by less demyelination. Progressively expanding demyelination in the absence of IL-10 demonstrates a critical role of IL-10 in constraining lesion area.

Morphological differences in focal versus expanding lesions were examined in Epon embedded sections at day 31 p.i. (Fig. 3C,D). Demyelination was confined to relatively small areas at the outer perimeter of the WT spinal cord (Fig. 3C). Debris filled macrophage/microglia were not prominent
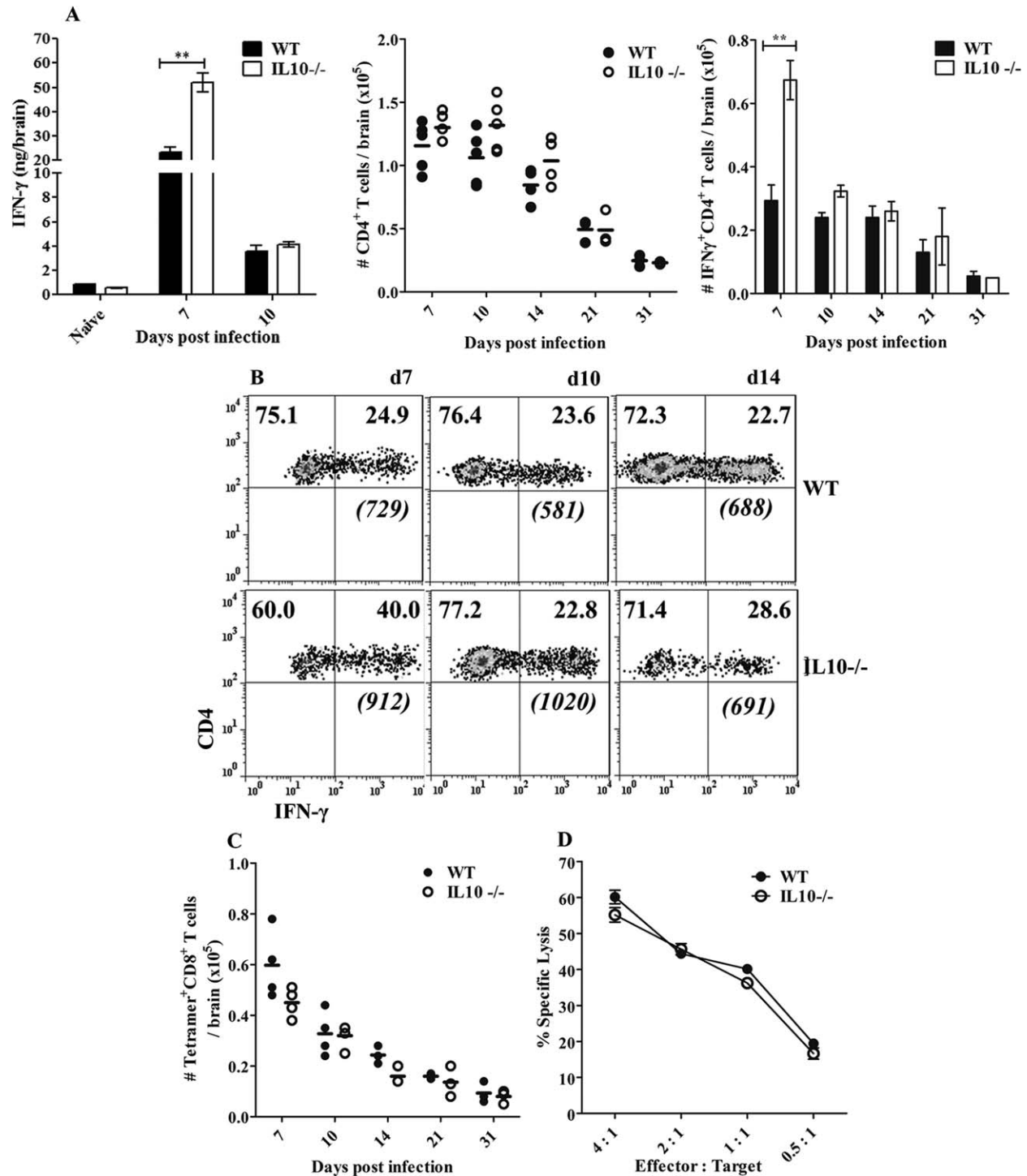
FIGURE 2: Enhanced CD4$^+$, but not CD8$^+$ T cell effector function in the absence of IL-10. (A) IFN-γ in brain supernatants determined by ELISA at indicated times p.i. Data expressed as mean ± SEM is representative of three separate experiments, with $n = 3$ per group at each point (Left Panel). Total numbers of CD4$^+$ T cells in brains of WT and IL-10$^{-/-}$ infected mice at various times p.i. Each data point represents an independent experiment with samples pooled from 3 to 4 mice per time point (Center Panel). Total numbers of virus specific IFN-γ secreting CD4$^+$ T cells in the CNS at various times p.i. Samples were pooled from 3-4 individuals per time point (Right Panel). (B) Flow cytometry depicting the percentage of CNS derived virus specific IFN-γ producing CD4$^+$ T cells at various times p.i. Italicized numbers in parenthesis represent the average IFN-γ mean fluorescent intensity (MFI). Data are representative of three independent experiments with cells pooled from 3 to 4 individuals per time point. Asterisks represent significant differences (**$P < 0.001$) as determined by unpaired, two-tailed, student's t test. (C) Virus specific CD8$^+$ T cell accumulation in the CNS of infected WT and IL-10$^{-/-}$ mice at various times p.i. Each data point represents an independent experiment with samples pooled from 3 to 4 mice per time point. (D) Cytolytic activity of virus specific CD8$^+$ T cells derived from the CNS of infected WT or IL-10$^{-/-}$ mice at day 7 p.i. Plot depicts percentage of specific lysis of S510-peptide pulsed target cells at various effector:target (E:T) ratios. Data represents mean ± SEM from two separate experiments with each sample pooled from 6 to 7 individuals.
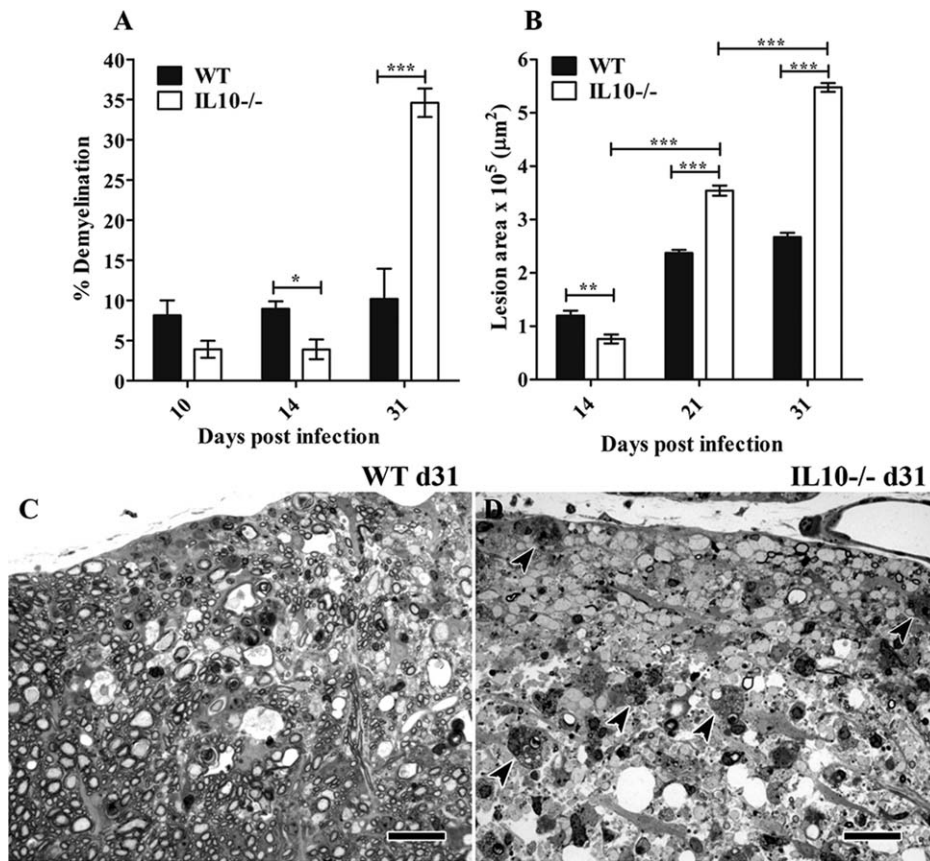
FIGURE 3: Enhanced demyelination in the absence of IL-10. **(A)** Percentage demyelination in LFB stained sections of spinal cord white matter in infected WT and IL-10$^{-/-}$ mice at various times p.i. Quantification based on transverse sections from 6 levels of each spinal cord. Data represents mean percentage ± SEM, with 5–6 spinal cords per time point. **(B)** Lesion areas based on immunohistochemical staining using anti-PLP in spinal cords of WT and IL-10$^{-/-}$ mice. Data represents mean ± SEM, with 7–9 spinal cords per time point. *$P < 0.05$, **$P < 0.001$, ***$P < 0.0001$ determined by unpaired, two-tailed, student's *t*-test. Demyelinated lesions in **(C)** WT and **(D)** IL-10$^{-/-}$ spinal cord segments at day 31 p.i. when examined in 1 micron Epon sections. Larger demyelinated lesions and debris laden phagocytic macrophage/microglia present in sections from IL-10$^{-/-}$ mice (D, arrowheads). Scale bar = 25 microns.

in these areas, indicating sparse active demyelination. Consistent with the lesion area determinations, demyelinated lesions were significantly larger in spinal cords from infected IL-10$^{-/-}$ mice (Fig. 3D). Moreover, the presence of phagocytic macrophage/microglia at the outer perimeter of the lesions (Fig. 3D, arrowheads) supported ongoing active demyelination, spreading from the perimeter toward the center of the spinal cord. In addition, the numbers of demyelinated axons were significantly increased in the IL-10$^{-/-}$ spinal cords.

Demyelination is Independent of Sustained T Cell Activation

Bystander damage due to uncontrolled and/or sustained T cell activation can contribute to pathology during viral infections of lung, mucosal sites as well as the CNS (Lund et al., 2008; Phares et al., 2010; Richards et al., 2011; Sun et al., 2009, 2011). However, there was no evidence for either altered recruitment of inflammatory cells into the brain (Fig.

1G) or mononuclear cells adjacent to, or within, demyelinating lesions in WT or IL-10$^{-/-}$ mice by histological examination (Fig. 1D,E). Irrespective of similar T cell recruitment into the brain (Fig. 2), we also compared the composition and frequency of T cells within spinal cords of infected WT and IL-10$^{-/-}$ mice to exclude the possibility that sustained inflammation contributed to increasing lesion area. CD4$^+$ T cells accumulated to similar maximal numbers between days 10 and 14 p.i. (Fig. 4A) and declined thereafter in both groups. Virus specific CD8$^+$ T cells in spinal cords accumulated between days 14 and 21 p.i. (Fig. 4B) reflecting similar, but preferential recruitment/retention at the site of viral persistence relative to brain. Similar to CD4$^+$ T cells there was no evidence of sustained CD8$^+$ T cell activation in spinal cords. IFN-γ mRNA expression was maximal at day 7 p.i. and ~5-fold higher in the absence of IL-10 (Fig. 4C), but declined to minimal detectable levels by day 21 p.i. in both groups. These data indicated that lesion expansion in the
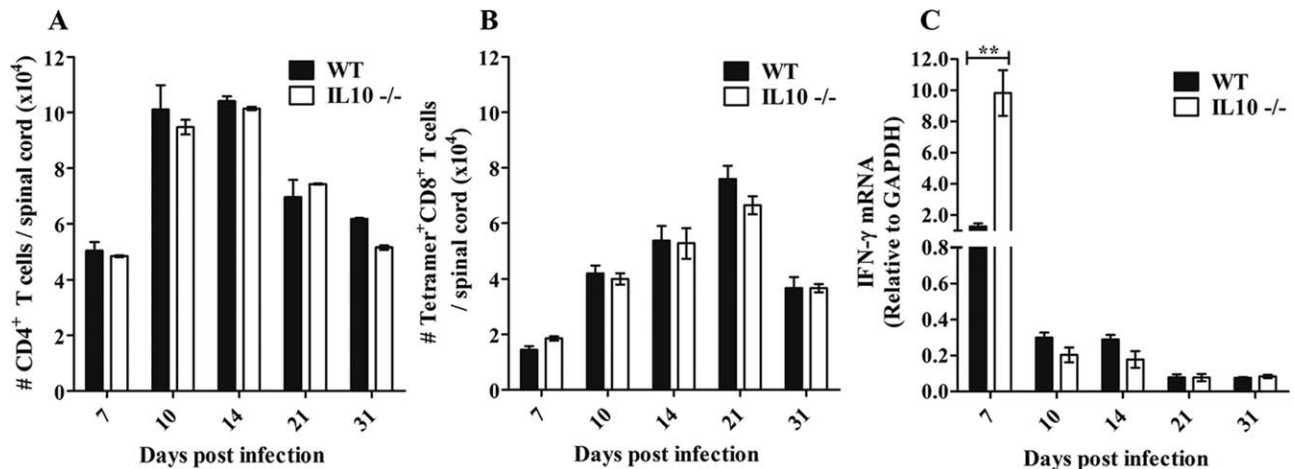
FIGURE 4: IL-10 does not regulate effector T cell recruitment but limits IFN-γ within spinal cord. (A) CD4$^+$ and (B) virus specific CD8$^+$ T cells in spinal cords of infected WT and IL-10$^{-/-}$ mice at various times p.i. Data are mean ± SEM of 2 separate experiments. (C) Expression of IFN-γ mRNA in spinal cords of infected WT and IL-10$^{-/-}$ mice. Data are representative of two separate experiments and expressed as mean ± SEM of three individuals per time point relative to GAPDH mRNA expression. **$P < 0.001$ determined by unpaired, two-tailed, student's t-test.

absence of IL-10 is independent of persisting virus levels or sustained T cell activity.

IL-10 Regulates Microglia/Macrophage Phenotype

Lesions in both WT and IL-10$^{-/-}$ groups were surrounded by microglia/macrophages with rounded cell bodies and withdrawn processes (Fig. 6), indicative of sustained activation. Although IL-10 is associated with an acquired deactivation phenotype (Mosser and Edwards, 2008), neither the relative expression of genes associated with repair following viral induced demyelination, nor the influence of IL-10 on these genes are well defined. To examine the influence of IL-10 on promoting a deactivation phenotype, we compared expression of CD206/mannose receptor associated with induction of deactivated macrophages (Martinez-Pomares, 2012). CD206 expressing cells were initially present in the lesions of WT mice; however, their number declined as inflammation declined and lesion size stabilized. Interestingly, CD206$^+$ cell numbers associated with lesions were increased in IL-10$^{-/-}$ relative to WT mice at day 14 p.i. (Fig. 5A–C), suggesting IL-10 independent CD206 induction. Subsequently however, CD206$^+$ cells declined in both groups to below the level of detection (Fig. 5C). Loss of the CD206$^+$ deactivation phenotype was thus not a marker for exacerbated tissue destruction in the absence of IL-10. Analysis of additional genes associated with the transitional decrease in activation showed that IL-1Ran mRNA expression in spinal cords was initially higher in IL10$^{-/-}$ as compared to WT mice but subsequently declined in both groups (Fig. 5D) with a more pronounced drop apparent in IL-10$^{-/-}$ mice. Arg-1 mRNA expression, initially reduced in the absence of IL-10, declined similarly

with time p.i., approaching naïve levels by day 31 p.i. (Fig. 5E). Additional markers of anti-inflammatory activation, i.e., Fizz1 and Ym1/2, were expressed at similar levels in the spinal cords of IL-10$^{-/-}$ and WT mice (data not shown). Despite similar inflammation and morphological evidence of microglia/macrophage activation (Fig. 1 and 2), initially reduced demyelination in IL-10$^{-/-}$ mice thus correlated with microglia/macrophages expressing an acquired deactivation phenotype, which was progressively lost, irrespective of lesion stability.

Expression of iNOS and MHC class II were examined to determine if increasing demyelination in the absence of IL-10 was associated with sustained microglial/macrophage activation. Consistent with stable foci of demyelination, few microglia/macrophages and <10% of astrocytes in the lesions of WT mice expressed iNOS (Fig. 6A–C, G) By contrast, ~40% of Iba1$^+$cells associated with lesions in IL-10$^{-/-}$ mice expressed iNOS (Fig. 6D–F, G), while iNOS$^+$ astrocytes were similar to WT mice. These data are consistent with retention of activated Iba1$^+$ cells during lesion expansion. Iba1$^+$ cells distal to the lesions did not express iNOS in either WT or IL-10$^{-/-}$ mice (data not shown). Similarly, while few MHC class II$^+$Iba1$^+$ cells were associated with focal lesions in WT mice (Fig. 6H–J, N), the majority of lesion associated Iba1$^+$ cells in IL-10$^{-/-}$ mice expressed MHC class II (Fig. 6K–M, N). By contrast, MHC class II$^+$Iba1$^+$ cells were not present in areas of normal white matter or within the adjoining gray matter in either group (data not shown). Demyelination in the absence of IL-10 was thus associated with microglia/macrophages expressing a sustained pro-inflammatory phenotype in contrast to the few pro-
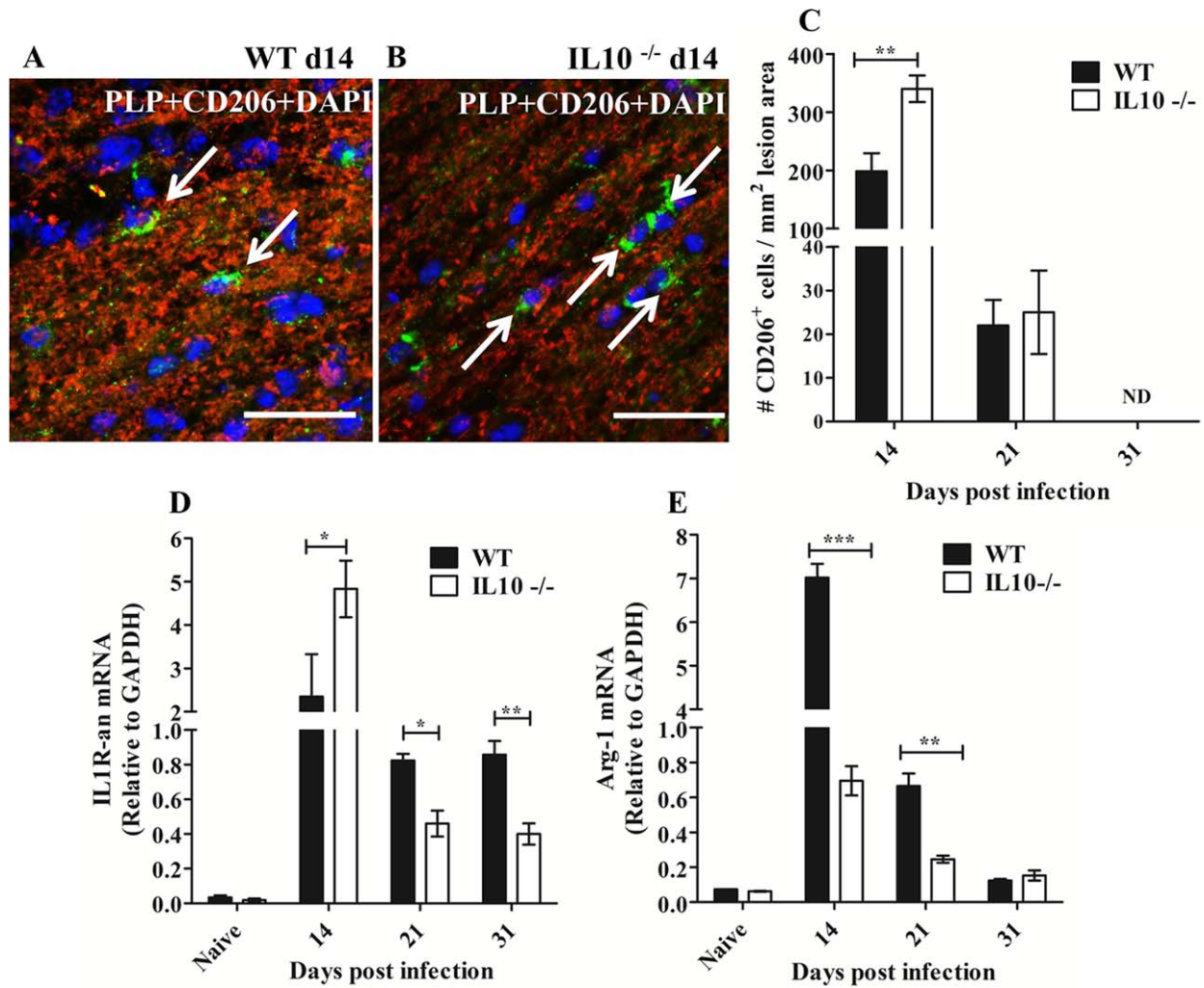
FIGURE 5: Loss of an acquired deactivation phenotype in the absence of IL-10. Spinal cords of infected (A) WT and (B) IL-10$^{-/-}$ mice at day 14 p.i. stained with anti-CD206 (green) and anti-PLP (red). Images are representative of three separate experiments with three individuals per group at each time point. Scale bar = 50 microns. (C) Number of lesion associated CD206$^+$ cells per mm^2 lesion area in WT and IL-10$^{-/-}$ mice. Data expressed as mean ± SEM are representative of three separate experiments using spinal cords from three individual mice per group at each time point. ND, not detected. Expression of (D) IL1 receptor antagonist (IL1Ran) and (E) Arginase 1 (Arg1) in spinal cords of infected WT and IL-10$^{-/-}$ mice at the indicated times p.i. Data are representative of two separate experiments and expressed as mean ± SEM of three individual spinal cords per time point and are relative to GAPDH mRNA expression. *$P < 0.05$, **$P < 0.001$, ***$P < 0.0001$ determined by unpaired, two-tailed, student's t-test.

inflammatory microglia/macrophages associated with the stable focal lesions in WT mice.

Influences of IL-10 deficiency on macrophages versus microglia in spinal cords were assessed by flow cytometry based on differential CD45 expression (Ford et al., 1995). Macrophages (CD45^{hi}CD11b$^+$) were initially increased at day 14 p.i. in IL-10$^{-/-}$ mice, but declined to similar numbers in both groups thereafter (Fig. 7A). The number of activated MHC class II$^+$ macrophages was similar at day 14 p.i. and decreased in both groups with a more pronounced drop in the absence of IL-10 (Fig. 7B,C). The number of microglia (CD45^{low}CD11b$^+$) remained relatively stable, independent of IL-10 (Fig. 7D). However, while the number of MHC class

II$^+$ microglia declined by ~50% in WT mice, microglia remained MHC class II$^+$ in the absence of IL-10 as lesion area increased (Fig. 7E,F), implicating microglia as the activated population of Iba1$^+$ cells associated with increasing lesion area (Fig. 6H–N).

Impaired Glial Scar Formation in the Absence of IL-10

The progressive expansion of demyelination in the absence of IL-10 is reminiscent of expanding lesions in the absence of astroglial scar formation following spinal cord injury and autoimmune mediated demyelination (Faulkner et al., 2004; Toft-Hansen et al., 2011; Voskuhl et al., 2009). Astrogliosis
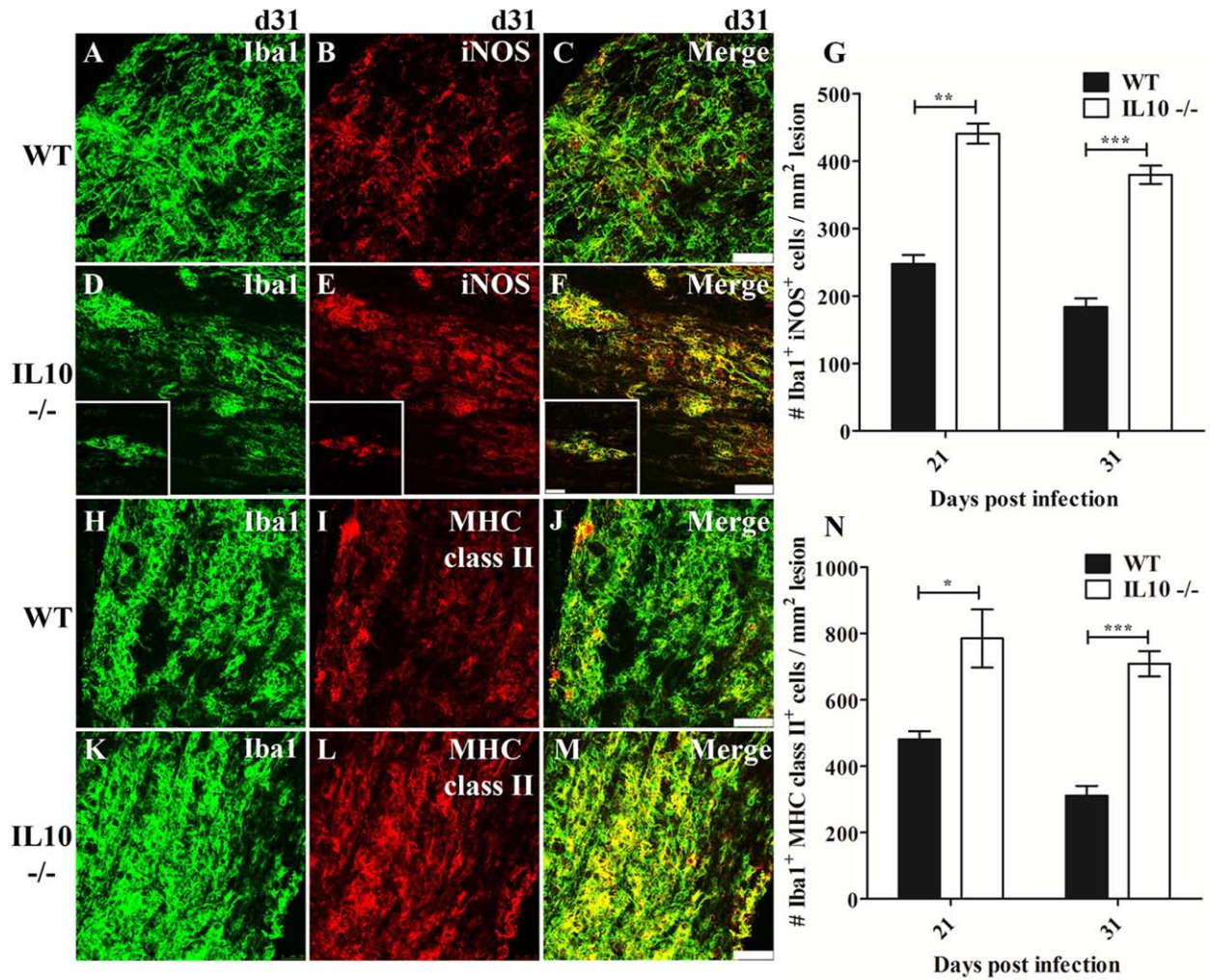
FIGURE 6: Sustained pro-inflammatory activation in the absence of IL-10. Iba$^+$ microglia/macrophages surrounding lesions in (**A and H**) WT and (**D&K**) IL-10$^{-/-}$ mice at day 31 p.i. iNOS$^+$ cells surrounding lesions in spinal cords from (**B**) WT and (**E**) IL-10$^{-/-}$ mice at day 31 p.i. Coexpression of Iba1 and iNOS surrounding lesions in (**C**) WT and (**F**) IL-10$^{-/-}$ mice at day 31 p.i. Scale bar = 250 microns, Inset scale bar = 50 microns (**G**). Total number of lesion associated Iba1$^+$ iNOS$^+$ cells/mm^2 lesion area in spinal cords of infected WT and IL-10$^{-/-}$ mice. MHC class II$^+$ cells surrounding lesions in (**I**) WT and (**L**) IL-10$^{-/-}$ spinal cords at day 31 p.i. Coexpression of Iba1 and MHC class II surrounding lesions in (**J**) WT and (**M**) IL-10$^{-/-}$ mice at day 31 p.i. Scale bar = 250 microns. Images are representative of three individual experiments using spinal cords from two individual mice per group. (**N**) Number of lesion associated Iba1$^+$MHC class II$^+$ cells per mm^2 lesion area in spinal cords of infected WT and IL-10$^{-/-}$ mice. Data are expressed as mean ± SEM and are representative of three individual experiments using spinal cords from two individual mice per group for each time point. *$P < 0.05$, **$P < 0.001$, ***$P < 0.0001$ determined by unpaired, two-tailed, student's t-test.

was thus analyzed by comparing the number and distribution of astrocytes associated with focal relative to expanding lesions. GFAP$^+$ astrocytes were present both at the edges and within lesions of WT mice (Fig. 8A–C,8G). Unlike the stellate morphology characteristic of resting astrocytes in uninvolved white matter (Fig. 8L), areas of myelin loss in WT mice exhibited increased GFAP expression and an organizational pattern consistent with scar-like structures (Fig. 8A–C). Furthermore, increasing astrocyte numbers per lesion area in WT mice from day 21 to 31 p.i. suggested an active repair response (Fig. 8G). By contrast, diffuse lesions in the absence

of IL-10 were devoid of organized astrocyte formations at the lesion edges and the numbers of activated astrocytes were decreased (Fig. 8D–F, G). Stable astrocyte numbers per lesion area in IL-10$^{-/-}$ mice supported a lack of proliferation due to the absence of IL-10 mediated STAT-3 signaling. This notion was supported by IL-10R induction on activated astrocytes associated with lesions (Fig. 8H–K), but not on astrocytes in surrounding uninvolved white matter (Fig. 8H, L–N). Indeed, no other cell type associated with the lesions including Iba1$^+$ macrophage/microglia or CD3$^+$ T cells expressed the IL-10R. Impaired astrocyte scar formation in
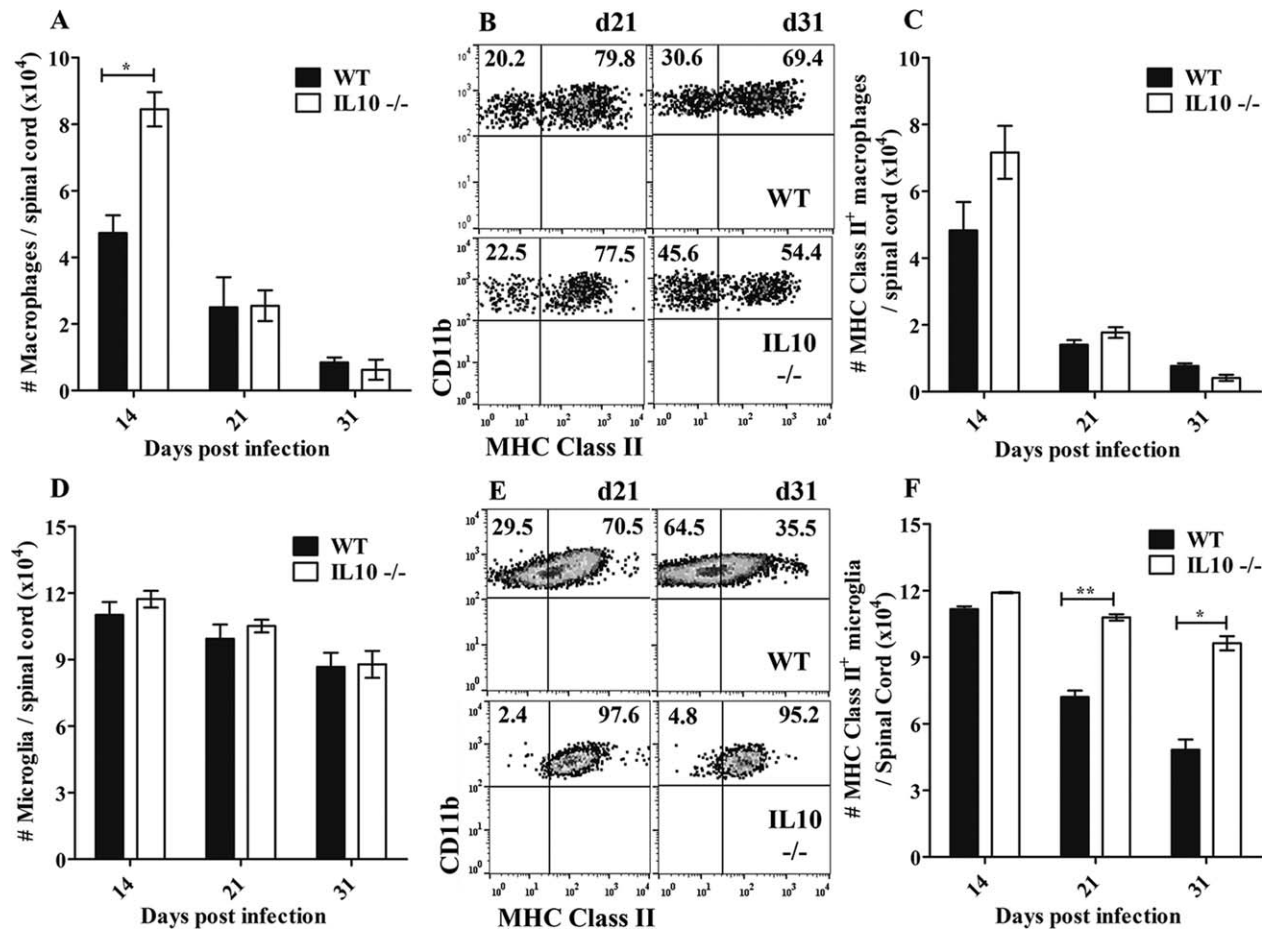
FIGURE 7: Sustained MHC class II expression by microglia in the absence of IL-10. Numbers of (A) CD11b$^+$CD45^{hi} macrophages and (D) CD11b$^+$CD45$^{low/int}$ microglia in WT and IL-10$^{-/-}$ spinal cords at the indicated times p.i. MHC class II$^+$ cells within (B) CD11b$^+$CD45^{hi} macrophages and (E) CD11b$^+$CD45^{low} microglia at days 21 and 31 p.i. determined by flow cytometry. Numbers indicate percentages within respective quadrants. Cells were pooled from spinal cords of 3–4 individual mice per time point. Data are representative of two separate experiments with similar results. Total number of (C) MHC class II$^+$ macrophages and (F) MHC class II$^+$ microglia within spinal cords at indicated times p.i. Data are mean ± SEM of two separate experiments. *$P < 0.05$, **$P < 0.001$ determined by unpaired, two-tailed, student's t-test.

the absence of IL-10 indicated that IL-10 confines focal lesions following viral induced demyelination via altering astrogliosis.

Discussion

The anti-inflammatory properties of IL-10 are known to dampen T cell effector function (Couper et al., 2008a; Fahey and Brooks, 2010). However, the relative contribution of reduced T cell activity versus additional IL-10 mediated regulation of tissue resident cells to CNS pathology is less well explored. The data herein support the concept that IL-10 plays three distinct, yet overlapping roles in the JHMV model of viral induced demyelination. First, it selectively dampens CD4$^+$ T cell IFN-γ production, thereby delaying viral control and enhancing initial demyelination. Second, by limiting IFN-γ, IL-10 not only deactivates microglia/macrophages but also dampens their pro-inflammatory responses. Third, IL-10

signaling facilitates glial scar formation by astrocytes thus containing lesion size. The anti-inflammatory consequences of IL-10 signaling in initially increasing demyelination are thus counterbalanced by a repair promoting activity apparent in microglia/macrophages as well as astrocytes. This in turn prevents lesion spread independent of residual persisting virus and sustained T cell mediated inflammation.

CD4$^+$ T cells are the major source of IL-10 within the CNS during JHMV induced encephalomyelitis (Puntambekar et al., 2011), implicating either Foxp3$^+$ regulatory T cells (Treg) or IL-27 induced Type 1 regulatory (Tr1) T cells as the IL-10 producing populations, which suppress IFN-γ production. Moreover, IL-10 selectively suppressed effector CD4$^+$ T cells, as neither CD8$^+$ T cell IFN-γ production nor cytolytic activity was altered in the absence of IL-10. The absence of an effect on cytolysis is distinct from increased cytolytic activity associated with a subpopulation of IL-10
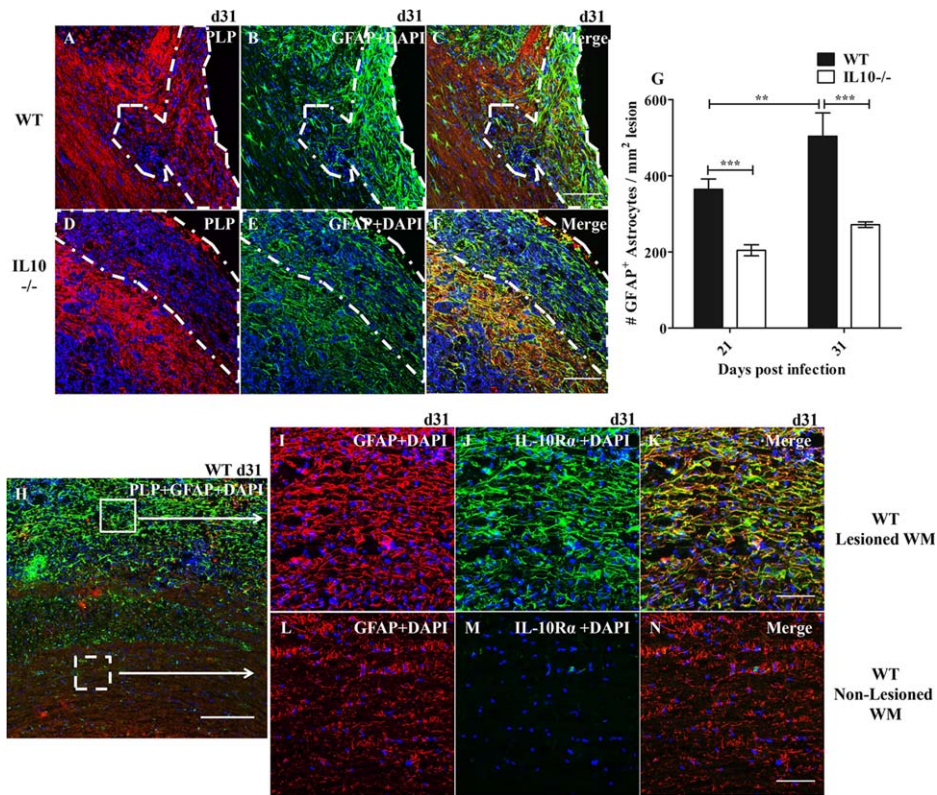
FIGURE 8: IL-10 regulates astroglial scar formation. Demyelinating lesions in spinal cords defined by staining for PLP and GFAP$^+$ astrocytes at day 31 p.i. in infected (A–C) WT and (D–F) IL-10$^{-/-}$ mice. Dashed lines delineate lesions used to quantify lesion area and the number of lesion associated GFAP$^+$ astrocytes. Scale bar = 200 microns. (G) GFAP$^+$ astrocytes per mm^2 lesion area in infected WT and IL-10$^{-/-}$ mice. Data expressed as mean ± SEM and are representative of three individual experiments using spinal cords from two individuals per group for each time point. **$P < 0.001$, ***$P < 0.0001$ determined by unpaired, two-tailed, student's t-test. (H) WT spinal cord showing GFAP$^+$ astrocytes (green) in lesioned (solid box) and nonlesioned (dashed box) white matter defined by staining for PLP (red). Scale bar = 400 microns. (I–K) IL-10R expression by GFAP$^+$ astrocytes surrounding lesioned white matter in infected WT mice at day 31 p.i. (L–N) IL-10R expression by GFAP$^+$ astrocytes in normal appearing white matter distal from the lesion in spinal cords from infected WT mice at day 31 p.i. Scale bar = 100 microns.

expressing virus specific CD8$^+$ T cells (Trandem et al., 2011). Both IL-10 producing Treg and Tr1 cells are rapidly recruited into the CNS following JHMV infection, do not alter CNS inflammation, and decline but are sustained throughout persistence (Anghelina et al., 2009; de Aquino et al., 2013, 2014). Adoptive transfer and depletion studies suggest distinct roles of Treg and Tr1 cells in suppressing antiviral activity versus demyelination. Treg transfer during acute JHMV infection ameliorated clinical disease and immunopathology without altering viral clearance (Trandem et al., 2010). Similarly, Treg depletion during acute infection only transiently impaired infectious virus control coincident with a minimal increase in demyelination (de Aquino et al., 2013). By contrast, elimination of Tr1 cells during JHMV infection accelerated viral clearance and reduced demyelination (de Aquino et al., 2014). These data suggested that Tr1 cells are not the IL-10 source during chronic infection preventing sustained demyelination, contrasting with the results of CNS pathology mediated by parasites and autoimmune disease

(Butler et al., 2013; Pot et al., 2011). Our data cannot rule out the possibility that the early increase in IFN-γ inflicts increased and irreversible oxidative damage in the absence of IL-10 (Molina-Holgado et al., 2001), which is progressively manifested at later time points. However, the similar increase in IFN-γ coupled with reduced demyelination in the absence of Tr1 cells (de Aquino et al., 2014) supports to the concept that Tr1 cells are not the source of IL-10 preventing sustained demyelination.

JHMV induced demyelination requires both infection of oligodendroglia and antiviral cell mediated immunity (Bergmann et al., 2004; Wu et al., 2000). The lesions are defined by a mixed population of macrophages and microglia expressing both pro-inflammatory and repair promoting genes, similar to lesion formation after spinal cord injury (Kigerl et al., 2009). However, the highly polarized Th1 immune response to JHMV coincides with only sparse IL-4 and IL-13 expression, preempting the transition to, or replacement of pro-inflammatory macrophages by an IL-4/IL-

13 dependent repair-promoting phenotype evident following peripheral injury (Chen et al., 2012; Shirey et al., 2010). The limited induction of IL-4/IL-13 dependent populations nevertheless appears to be compensated by transition to an IL-10 dependent anti-inflammatory microglia/macrophage phenotype, which augments remyelination through enhanced phagocytosis/clearance of myelin debris and/or oligodendrogenesis (Butovsky et al., 2006; Miron et al., 2013). The CNS lesion micro-environment associated with IL-10 thus appears to ellicit a unique repair promoting microglia/macrophage phenotype, which restrains by-stander immune pathology. Our data indicate that impaired activation of cells that support tissue repair in the absence of IL-10, combined with persistent pro-inflammatory activation and the lack of a clear transition to an anti-inflammatory phenotype contributes to progressive myelin loss. JHMV induced demyelination shares a variety of pathophysiological features with MS and EAE, but differs in two important aspects. First, the highly polarized Th1 response excludes T cells secreting IL-17 (Kapil et al., 2009; Savarin et al., 2012). Second, viral induced demyelination is independent of bone marrow derived macrophages (Savarin et al., 2010; Xue et al., 1999). This is supported by the continuous decline in activated macrophages within spinal cords in both infected WT and IL-10$^{-/-}$ mice as well as sustained microglial, but not macrophage activation associated with the expanding lesions in the absence of IL-10. This contrasts the concerted effort of macrophages stripping myelin with microglia phagocytizing myelin debris during EAE (Yamasaki et al., 2014). Pathologically similar tissue damage, i.e., demyelination, can thus be affected by distinct mechanisms during viral and autoimmune induced lesion formation. Irrespectively, the focal nature of demyelination following distinct CNS insults, many of which are associated with increased IL-10 (Weiner and Selkoe, 2002), support a conserved mechanism that involves astrocyte activation and glial scar formation to limit CNS damage (Cregg et al., 2014; Sofroniew and Vinters, 2010). Focal demyelinated lesions are characterized by increased expression of GFAP indicative of an astrogliotic scar (Silver and Miller, 2004). Induction of EAE in GFAP$^{-/-}$ mice (Liedtke et al., 1998) or ablation of proliferating astrocytes supports the critical role of astrogliosis in the formation of discrete white matter lesions and the concept that astrocytes not only regulate glial scar formation, but also limit inflammatory cell invasion into the CNS parenchyma (Toft-Hansen et al., 2011; Voskuhl et al., 2009).

A universal role of IL-10 in white matter lesion formation is supported by focal IL-10R expression by activated astrocytes, coincident with suppressed microglia activation in rodent models of both MS and CNS injury (Hulshof et al., 2002; Ledeboer et al., 2003; Starossom et al., 2012; Xin et al., 2011). Moreover, by binding their respective receptors,

IL-10, IL-6, LIF, and CNTF all activate STAT3 (Schindler et al., 2007), supporting a contribution of IL-10 induced STAT3 activation to the formation of focal lesions following viral induced demyelination. Indeed, in a spinal cord injury model, STAT3 ablation specifically in astrocytes resulted in lesion expansion, coincident with inhibited astrocyte migration and formation of a distinct lesion border, as well as increased macrophage infiltration (Wanner et al., 2013). A critical role of STAT3 signaling in regulating astrocyte function is also supported by spinal cord injury in mice in which SOCS3, which inhibits STAT3 signaling, was specifically ablated in astrocytes. Conditional disruption of SOCS3 signaling increased astrocyte migration, lesion confinement and functional recovery (Okada et al., 2006). The present data thus expand the regulation of autoimmune mediated demyelination and spinal cord injury by restricted expression of IL-10R and potential STAT3 signaling in astrocytes, to include viral induced demyelination. Lesion expansion, despite accelerated clearance of a subacute viral infection, is further reminiscent of epidemiological data implicating an elusive environmental agent in the pathophysiology of MS (Fujinami et al., 2006). Overall this model defines multifactorial events by which IL-10 limits CNS damage subsequent to viral control and supports the concept that IL-10 signaling to astrocytes regulates the formation of the glial scar surrounding and limiting areas of demyelination.

References

Anghelina D, Zhao J, Trandem K, Perlman S. 2009. Role of regulatory T cells in coronavirus-induced acute encephalitis. Virology 385:358–367.

Barnett MH, Prineas JW. 2004. Relapsing and remitting multiple sclerosis: Pathology of the newly forming lesion. Ann Neurol 55:458–468.

Bender SJ, Weiss SR. 2010. Pathogenesis of murine coronavirus in the central nervous system. J Neuroimmune Pharmacol 5:336–354.

Bergmann CC, Altman JD, Hinton D, Stohlman SA. 1999. Inverted immunodominance and impaired cytolytic function of CD8+ T cells during viral persistence in the central nervous system. J Immunol 163:3379–3387.

Bergmann CC, Lane TE, Stohlman SA. 2006. Coronavirus infection of the central nervous system: Host-virus stand-off. Nat Rev Microbiol 4:121–132.

Bergmann CC, Parra B, Hinton DR, Ramakrishna C, Dowdell KC, Stohlman SA. 2004. Perforin and gamma interferon-mediated control of coronavirus central nervous system infection by CD8 T cells in the absence of CD4 T cells. J Virol 78:1739–1750.

Butler NS, Harris TH, Blader IJ. 2013. Regulation of immunopathogenesis during Plasmodium and Toxoplasma infections: More parallels than distinctions? Trends Parasitol 29:593–602.

Butovsky O, Landa G, Kunis G, Ziv Y, Avidan H, Greenberg N, Schwartz A, Smirnov I, Pollack A, Jung S, Schwartz M. 2006. Induction and blockage of oligodendrogenesis by differently activated microglia in an animal model of multiple sclerosis. J Clin Invest 116:905–915.

Couper KN, Blount DG, Riley EM. 2008a. IL-10: the master regulator of immunity to infection. J Immunol 180:5771–5777.

Couper KN, Blount DG, Wilson MS, Hafalla JC, Belkaid Y, Kamanaka M, Flavell RA, de Souza JB, Riley EM. 2008b. IL-10 from CD4CD25Foxp3CD127

adaptive regulatory T cells modulates parasite clearance and pathology during malaria infection. PLoS Pathog 4:e1000004.

Cregg JM, DePaul MA, Filous AR, Lang BT, Tran A, Silver J. 2014. Functional regeneration beyond the glial scar. Exp Neurol 253:197–207.

Chen F, Liu Z, Wu W, Rozo C, Bowdridge S, Millman A, Van Rooijen N, Urban JF Jr, Wynn TA, Gause WC. 2012. An essential role for TH2-type responses in limiting acute tissue damage during experimental helminth infection. Nat Med 18:260–266.

de Aquino MT, Kapil P, Hinton DR, Phares TW, Puntambekar SS, Savarin C, Bergmann CC, Stohlman SA. 2014. IL-27 limits central nervous system viral clearance by promoting IL-10 and enhances demyelination. J Immunol 193:285–294.

de Aquino MT, Puntambekar SS, Savarin C, Bergmann CC, Phares TW, Hinton DR, Stohlman SA. 2013. Role of CD25(+) CD4(+) T cells in acute and persistent coronavirus infection of the central nervous system. Virology 447:112–120.

Fahey LM, Brooks DG. 2010. Opposing positive and negative regulation of T cell activity during viral persistence. Curr Opin Immunol 22:348–354.

Faulkner JR, Herrmann JE, Woo MJ, Tansey KE, Doan NB, Sofroniew MV. 2004. Reactive astrocytes protect tissue and preserve function after spinal cord injury. J Neurosci 24:2143–2155.

Fleming JO, Trousdale MD, el-Zaatari FA, Stohlman SA, Weiner LP. 1986. Pathogenicity of antigenic variants of murine coronavirus JHM selected with monoclonal antibodies. J Virol 58:869–875.

Ford AL, Goodsall AL, Hickey WF, Sedgwick JD. 1995. Normal adult ramified microglia separated from other central nervous system macrophages by flow cytometric sorting. Phenotypic differences defined and direct ex vivo antigen presentation to myelin basic protein-reactive CD4+ T cells compared. J Immunol 154:4309–4321.

Fujinami RS, von Herrath MG, Christen U, Whitton JL. 2006. Molecular mimicry, bystander activation, or viral persistence: infections and autoimmune disease. Clin Microbiol Rev 19:80–94.

Herrmann JE, Imura T, Song B, Qi J, Ao Y, Nguyen TK, Korsak RA, Takeda K, Akira S, Sofroniew MV. 2008. STAT3 is a critical regulator of astrogliosis and scar formation after spinal cord injury. J Neurosci 28:7231–7243.

Holscher C, Mohrs M, Dai WJ, Kohler G, Ryffel B, Schaub GA, Mossmann H, Brombacher F. 2000. Tumor necrosis factor alpha-mediated toxic shock in Trypanosoma cruzi-infected interleukin 10-deficient mice. Infect Immun 68:4075–4083.

Hulshof S, Montagne L, De Groot CJ, Van Der Valk P. 2002. Cellular localization and expression patterns of interleukin-10, interleukin-4, and their receptors in multiple sclerosis lesions. Glia 38:24–35.

Kapil P, Atkinson R, Ramakrishna C, Cua DJ, Bergmann CC, Stohlman SA. 2009. Interleukin-12 (IL-12), but not IL-23, deficiency ameliorates viral encephalitis without affecting viral control. J Virol 83:5978–5986.

Kapil P, Butchi NB, Stohlman SA, Bergmann CC. 2012. Oligodendroglia are limited in type I interferon induction and responsiveness in vivo. Glia 60:1555–1566.

Kigerl KA, Gensel JC, Ankeny DP, Alexander JK, Donnelly DJ, Popovich PG. 2009. Identification of two distinct macrophage subsets with divergent effects causing either neurotoxicity or regeneration in the injured mouse spinal cord. J Neurosci 29:13435–13444.

Kulcsar KA, Baxter VK, Greene IP, Griffin DE. 2014. Interleukin 10 modulation of pathogenic Th17 cells during fatal alphavirus encephalomyelitis. Proc Natl Acad Sci U S A 111:16053–16058.

Kullberg MC, Jankovic D, Gorelick PL, Caspar P, Letterio JJ, Cheever AW, Sher A. 2002. Bacteria-triggered CD4(+) T regulatory cells suppress Helicobacter hepaticus-induced colitis. J Exp Med 196:505–515.

Ledeboer A, Wierinckx A, Bol JG, Floris S, Renardel de Lavalette C, De Vries HE, van den Berg TK, Dijkstra CD, Tilders FJ, van dam AM. 2003. Regional and temporal expression patterns of interleukin-10, interleukin-10 receptor and adhesion molecules in the rat spinal cord during chronic relapsing EAE. J Neuroimmunol 136:94–103.

Liedtke W, Edelmann W, Chiu FC, Kucherlapati R, Raine CS. 1998. Experimental autoimmune encephalomyelitis in mice lacking glial fibrillary acidic protein is characterized by a more severe clinical course and an infiltrative central nervous system lesion. Am J Pathol 152:251–259.

Lin MT, Hinton DR, Marten NW, Bergmann CC, Stohlman SA. 1999. Antibody prevents virus reactivation within the central nervous system. J Immunol 162:7358–7368.

Lin MT, Hinton DR, Parra B, Stohlman SA, van der Veen RC. 1998. The role of IL-10 in mouse hepatitis virus-induced demyelinating encephalomyelitis. Virology 245:270–280.

Lund JM, Hsing L, Pham TT, Rudensky AY. 2008. Coordination of early protective immunity to viral infection by regulatory T cells. Science 320:1220–1224.

Martinez-Pomares L. 2012. The mannose receptor. J Leuk Biol 92:1177–1186.

Metz L, Bell R, Zochodne D. 1994. Interferon beta treatment of multiple sclerosis. Neurology 44:187–188.

Miron VE, Boyd A, Zhao JW, Yuen TJ, Ruckh JM, Shadrach JL, van Wijngaarden P, Wagers AJ, Williams A, Franklin RJ, ffrench-Constant C. 2013. M2 microglia and macrophages drive oligodendrocyte differentiation during CNS remyelination. Nat Neurosci 16:1211–1218.

Molina-Holgado E, Vela JM, Arevalo-Martin A, Guaza C. 2001. LPS/IFN-gamma cytotoxicity in oligodendroglial cells: Role of nitric oxide and protection by the anti-inflammatory cytokine IL-10. Eur J Neurosci 13:493–502.

Mosser DM, Edwards JP. 2008. Exploring the full spectrum of macrophage activation. Nat Rev Immunol 8:958–969.

Okada S, Nakamura M, Katoh H, Miyao T, Shimazaki T, Ishii K, Yamane J, Yoshimura A, Iwamoto Y, Toyama Y, Okano H. 2006. Conditional ablation of Stat3 or Socs3 discloses a dual role for reactive astrocytes after spinal cord injury. Nat Med 12:829–834.

Parra B, Hinton DR, Marten NW, Bergmann CC, Lin MT, Yang CS, Stohlman SA. 1999. IFN-gamma is required for viral clearance from central nervous system oligodendroglia. J Immunol 162:1641–1647.

Phares TW, DiSano KD, Stohlman SA, Bergmann CC. 2014. Progression from IgD+ IgM+ to isotype-switched B cells is site specific during coronavirus-induced encephalomyelitis. J Virol 88:8853–8867.

Phares TW, Stohlman SA, Hinton DR, Atkinson R, Bergmann CC. 2010. Enhanced antiviral T cell function in the absence of B7-H1 is insufficient to prevent persistence but exacerbates axonal bystander damage during viral encephalomyelitis. J Immunol 185:5607–5618.

Pot C, Apetoh L, Kuchroo VK. 2011. Type 1 regulatory T cells (Tr1) in autoimmunity. Semin Immunol 23:202–208.

Puntambekar SS, Bergmann CC, Savarin C, Karp CL, Phares TW, Parra GI, Hinton DR, Stohlman SA. 2011. Shifting hierarchies of interleukin-10-producing T cell populations in the central nervous system during acute and persistent viral encephalomyelitis. J Virol 85:6702–6713.

Ramakrishna C, Bergmann CC, Atkinson R, Stohlman SA. 2003. Control of central nervous system viral persistence by neutralizing antibody. J Virol 77:4670–4678.

Ramakrishna C, Stohlman SA, Atkinson RD, Shlomchik MJ, Bergmann CC. 2002. Mechanisms of central nervous system viral persistence: the critical role of antibody and B cells. J Immunol 168:1204–1211.

Richards MH, Getts MT, Podojil JR, Jin YH, Kim BS, Miller SD. 2011. Virus expanded regulatory T cells control disease severity in the Theiler's virus mouse model of MS. J Autoimmun 36:142–154.

Saraiva M, O'Garra A. 2010. The regulation of IL-10 production by immune cells. Nat Rev Immunol 10:170–181.

Savarin C, Stohlman SA, Atkinson R, Ransohoff RM, Bergmann CC. 2010. Monocytes regulate T cell migration through the glia limitans during acute viral encephalitis. J Virol 84:4878–4888.

Savarin C, Stohlman SA, Hinton DR, Ransohoff RM, Cua DJ, Bergmann CC. 2012. IFN-gamma protects from lethal IL-17 mediated viral encephalomyelitis independent of neutrophils. J Neuroinflammation 9:104.

Schindler C, Levy DE, Decker T. 2007. JAK-STAT signaling: From interferons to cytokines. J Biol Chem 282:20059–20063.

Shirey KA, Pletneva LM, Puche AC, Keegan AD, Prince GA, Blanco JC, Vogel SN. 2010. Control of RSV-induced lung injury by alternatively activated macrophages is IL-4R alpha-, TLR4-, and IFN-beta-dependent. Mucosal Immunol 3:291–300.

Silver J, Miller JH. 2004. Regeneration beyond the glial scar. Nat Rev Neurosci 5:146–156.

Sofroniew MV, Vinters HV. 2010. Astrocytes: Biology and pathology. Acta Neuropathol 119:7–35.

Starossom SC, Mascanfroni ID, Imitola J, Cao L, Raddassi K, Hernandez SF, Bassil R, Croci DO, Cerliani JP, Delacour D, Wang Y, Elyaman W, Khoury SJ, Rabinovich GA. 2012. Galectin-1 deactivates classically activated microglia and protects from inflammation-induced neurodegeneration. Immunity 37: 249–263.

Stohlman SA, Hinton DR, Parra B, Atkinson R, Bergmann CC. 2008. CD4 T cells contribute to virus control and pathology following central nervous system infection with neurotropic mouse hepatitis virus. J Virol 82:2130–2139.

Sun J, Cardani A, Sharma AK, Laubach VE, Jack RS, Muller W, Braciale TJ. 2011. Autocrine regulation of pulmonary inflammation by effector T-cell derived IL-10 during infection with respiratory syncytial virus. PLoS Pathog 7: e1002173.

Sun J, Madan R, Karp CL, Braciale TJ. 2009. Effector T cells control lung inflammation during acute influenza virus infection by producing IL-10. Nat Med 15:277–284.

Templeton SP, Kim TS, O'Malley K, Perlman S. 2008. Maturation and localization of macrophages and microglia during infection with a neurotropic murine coronavirus. Brain Pathol 18:40–51.

Toft-Hansen H, Fuchtbauer L, Owens T. 2011. Inhibition of reactive astrocytosis in established experimental autoimmune encephalomyelitis favors infiltration by myeloid cells over T cells and enhances severity of disease. Glia 59: 166–176.

Trandem K, Anghelina D, Zhao J, Perlman S. 2010. Regulatory T cells inhibit T cell proliferation and decrease demyelination in mice chronically infected with a coronavirus. J Immunol 184:4391–4400.

Trandem K, Zhao J, Fleming E, Perlman S. 2011. Highly activated cytotoxic CD8 T cells express protective IL-10 at the peak of coronavirus-induced encephalitis. J Immunol 186:3642–3652.

Voskuhl RR, Peterson RS, Song B, Ao Y, Morales LB, Tiwari-Woodruff S, Sofroniew MV. 2009. Reactive astrocytes form scar-like perivascular barriers to leukocytes during adaptive immune inflammation of the CNS. J Neurosci 29:11511–11522.

Wang FI, Hinton DR, Gilmore W, Trousdale MD, Fleming JO. 1992. Sequential infection of glial cells by the murine hepatitis virus JHM strain (MHV-4) leads to a characteristic distribution of demyelination. Lab Invest 66:744–754.

Wanner IB, Anderson MA, Song B, Levine J, Fernandez A, Gray-Thompson Z, Ao Y, Sofroniew MV. 2013. Glial scar borders are formed by newly proliferated, elongated astrocytes that interact to corral inflammatory and fibrotic cells via STAT3-dependent mechanisms after spinal cord injury. J Neurosci 33:12870–12886.

Weiner HL, Selkoe DJ. 2002. Inflammation and therapeutic vaccination in CNS diseases. Nature 420:879–884.

Wu GF, Dandekar AA, Pewe L, Perlman S. 2000. CD4 and CD8 T cells have redundant but not identical roles in virus-induced demyelination. J Immunol 165:2278–2286.

Xin J, Wainwright DA, Mesnard NA, Serpe CJ, Sanders VM Jones KJ. 2011. IL-10 within the CNS is necessary for CD4+ T cells to mediate neuroprotection. Brain Behav Immun 25:820–829.

Xue S, Sun N, Van Rooijen N, Perlman S. 1999. Depletion of blood-borne macrophages does not reduce demyelination in mice infected with a neurotropic coronavirus. J Virol 73:6327–6334.

Yamasaki R, Lu H, Butovsky O, Ohno N, Rietsch AM, Cialic R, Wu PM, Doykan CE, Lin J, Cotleur AC, Kidd G, Zorlu MM, Sun N, Hu W, Liu L, Lee JC, Taylor SE, Uehlein L, Dixon D, Gu J, Floruta CM, Zhu M, Charo IF, Weiner HL, Ransohoff R. 2014. Differential roles of microglia and monocytes in the inflamed central nervous system. J Exp Med 211:1533–1549.